Published in final edited form as:
Bioconjug Chem. 2011 March 16; 22(3): 413–421. doi:10.1021/bc100432h.

Radiolabeled Affibody-Albumin Bioconjugates for *HER2* Positive Cancer Targeting

Susan Hoppmann[†], **Zheng Miao**[†], **Shuanglong Liu**[†], **Hongguang Liu**[†], **Gang Ren**[†], **Ande Bao**[‡], and **Zhen Cheng**[†,*]

[†] Molecular Imaging Program at Stanford (MIPS), Department of Radiology and Bio-X Program, Stanford University, Stanford, California, 94305

[‡] Departments of Radiology and Otolaryngology – Head and Neck Surgery, University of Texas Health Science Center at San Antonio, San Antonio, TX 78229

Abstract

Affibody molecules have received significant attention in the fields of molecular imaging and drug development. However, Affibody scaffolds display an extremely high renal uptake, especially when modified with chelators and then labeled with radiometals. This unfavorable property may impact their use as radiotherapeutic agents in general and as imaging probes for the detection of tumors adjacent to kidneys in particular. Herein, we present a simple and generalizable strategy for reducing the renal uptake of Affibody molecules while maintaining their tumor uptake. Human serum albumin (HSA) was consecutively modified by 1,4,7,10-Tetraazacyclododecane-1,4,7,10-tetraacetic acid mono-N-hydroxysuccinimide ester (DOTA-NHS ester) and the bifunctional crosslinker sulfosuccinimidyl 4-[*N*-maleimidomethyl]cyclohexane-1-carboxylate (Sulfo-SMCC). The *HER2* Affibody analog, Ac-Cys-$Z_{HER2:342}$, was covalently conjugated with HSA, and the resulting bioconjugate DOTA-HSA-$Z_{HER2:342}$ was further radiolabeled with ^{64}Cu and ^{111}In and evaluated *in vitro* and *in vivo*. Radiolabeled DOTA-HSA-$Z_{HER2:342}$ conjugates displayed a significant and specific cell uptake into SKOV3 cell cultures. Positron emission tomography (PET) investigations using ^{64}Cu-DOTA-HSA-$Z_{HER2:342}$ were performed in SKOV3 tumor-bearing nude mice. High tumor uptake values (> 14% ID/g at 24 h and 48 h) and high liver accumulations but low kidney accumulations were observed. Biodistribution studies and single-photon emission computed tomography (SPECT) investigations using ^{111}In-DOTA-HSA-$Z_{HER2:342}$ validated these results. At 24 h post injection, the bio distribution data revealed high tumor (16.26% ID/g) and liver uptake (14.11% ID/g) but relatively low kidney uptake (6.06% ID/g). Blocking studies with co-injected, non-labeled Ac-Cys-$Z_{HER2:342}$ confirmed the *in vivo* specificity of *HER2*. Radiolabeled DOTA-HSA-$Z_{HER2:342}$ Affibody conjugates are promising SPECT and PET-type probes for the imaging of *HER2* positive cancer. More importantly, DOTA-HSA-$Z_{HER2:342}$ is suitable for labeling with therapeutic radionuclides (e.g. ^{90}Y or ^{177}Lu) for treatment studies. The approach of using HSA to optimize the pharmacokinetics and biodistribution profile of Affibodies, may be extended to the design of many other targeting molecules.

INTRODUCTION

Recent years have seen substantial advances in the development of molecular-targeted imaging as well as advances in the therapy of various types of cancers. The human

*Author to whom correspondence should be addressed: Zhen Cheng, Ph.D., Molecular Imaging Program at Stanford, Department of Radiology and Bio-X Program, Canary Center at Stanford for Cancer Early Detection, 1201 Welch Road, Lucas Expansion, P095, Stanford University, Stanford, CA 94305, 650-723-7866 (V), 650-736-7925(Fax), zcheng@stanford.edu.

epidermal growth factor receptor 2 (*HER2*) has been frequently detected in a wide range of human tumors including breast, ovarian, lung, and gastric cancers (1–3). Additionally, *HER2* is associated with reduced overall survival and increased aggressiveness of the disease. Therefore, targeting of the receptor is thought to be beneficial for cancer patients with *HER2* amplification.

Affibody molecules are engineered small proteins with 58-amino acid residues (~ 7 kDa) and a three- α-helical bundle structure, as derived from one of the IgG-binding domains of staphylococcal protein A (4). Recently they have received significant attention as protein scaffolds for the development of probes for tumor and for therapeutic agents (5–7). In particular, *HER2*-binding Affibody molecules have been successfully used in the imaging and radionuclide therapy of tumors (4,8–16). For example, the Affibody molecule $Z_{HER2:342}$ binds to *HER2* with a dissociation constant (K_d) of 22 pM (6), and it displays excellent in vivo visualization of *HER2* expressing tumor xenografts when labeled with a variety of radionuclides (8–10,12,17–24). However, besides the high and specific imaging contrast, chelator modified and radiometal-labeled Affibody proteins typically exhibit an extremely high renal uptake (more than 100 percent of the injected radioactivity per gram of tissue, % ID/g), which is unfavorable for the detection of tumors adjacent to the kidneys. More importantly, the high renal accumulation of the radiometal labeled Affibody molecules could result in very high radiation doses to the radiation sensitive kidneys and thus represents a critical concern for using Affibody molecules for radionuclide. therapy.

Human serum albumin (HSA[1]) is a 65 kDa protein that is abundant in the circulation and features low immunogenicity, high biocompatibility and excellent biodegradability. Because of its long circulation property, it has been used as a carrier for drug delivery in advanced clinical trials (25). The renal filtration of these HSA-drug bioconjugates is also substantially inhibited by the high molecular size of albumin, thereby enabling prolonged exposure of the target cells to the bioconjugates. In another study, integrin $\alpha_v\beta_3$-binding RGD peptide was conjugated with HSA to improve molecular probe pharmacokinetics and to prolong the probe circulation and tumor contrast (26).

Herein, we use HSA as an ideal platform for conjugation with Affibody proteins and radiometal chelators (Figure 1). The resulting Affibody-albumin hybrids are expected to display several unique properties such as: 1) improved pharmacokinetics in terms of a low renal accumulation due to the high molecular size of the conjugate, 2) improved tumor targeting ability because of the multimeric structure of the conjugate using high affinity Affibody ligands, and 3) improved blood circulation and tumor accumulation. We have developed a simple and generalizable strategy for chemically conjugating Affibody (Ac-Cys-$Z_{HER2:342}$) molecules and 1,4,7,10-tetraazacyclododecane-1,4,7,10-tetraacetic acid (DOTA) with HSA. To study the biodistribution and pharmacokinetic of these novel bioconjugates, the Affibody-HSA conjugates were radiolabeled with the PET radionuclide ^{64}Cu ($t_{1/2}$ = 12.7 h, $E_{\beta+}$ max = 656 keV, 17.4%) and the SPECT radionuclide ^{111}In [$t_{1/2}$ = 67.4 h; EC 849 keV (100%); γ 173 keV (89%), 247 keV (94%)], respectively. The biologic profiles of the resulting probes (^{64}Cu-DOTA-HSA-$Z_{HER2:342}$ and ^{111}In-DOTA-HSA-$Z_{HER2:342}$) were evaluated in ovarian carcinoma SKOV3 cells with a high expression of *HER2* (15–16) and in nude mice bearing subcutaneous SKOV3 tumors.

[1]**ABBREVIATIONS**

DOTA, 1,4,7,10-tetraazacyclododecane-1,4,7,10-tetraacetic acid; PET, positron emission tomography; SPECT, single-photon emission computed tomography, HPLC, high performance liquid chromatography; HSA, Human serum albumin, p.i., postinjection.

MATERIALS AND METHODS

General

The Affibody molecule Ac-Cys-$Z_{HER2:342}$ (Ac-CVDNKFNKEMRNAYWEIA LLPNLNNQQKRAFIRSLYDDPSQSANLLAEAKKLNDAQAPK) was synthesized and analyzed in the same way as described for the Ac-Cys-$Z_{EGFR:1907}$ (27). 1,4,7,10-Tetraazacyclododecane-1,4,7,10-tetraacetic acid mono-N-hydroxysuccinimide ester (DOTA-NHS ester) was obtained from Macrocyclics Inc. Sulfo-SMCC (Sulfosuccinimidyl 4-[*N*-maleimidomethyl]cyclohexane-1-carboxylate) was purchased from Thermo Fisher Scientific. Human serum albumin (HSA) and all other standard reagents were purchased from Sigma-Aldrich Chemical Co. $^{64}CuCl_2$ was provided by the Department of Medical Physics, University of Wisconsin at Madison. $^{111}InCl_3$ was purchased from PerkinElmer, Inc. The human ovarian cancer SKOV3 cell line was obtained from the American Type Tissue Culture Collection. Female athymic nude mice (nu/nu) were purchased from Charles River Laboratories. All other instruments [e.g., radioactive dose calibrator and matrix-assisted laser desorption/ionization time of flight mass spectrometry (MALDI-TOF-MS)] were the same as those previously reported (13).

Bioconjugation of HSA with DOTA and Ac-Cys-$Z_{HER2:342}$

First, HSA (5 mg) was conjugated with DOTA-NHS ester (3.78 mg) in 200μL of borate buffer (50 mM, pH 8.5) in a molar ratio of 1:100 for 2 h at 4 °C (Figure 2). The resulting HSA-DOTA conjugate was then purified using a PD-10 column (GE Healthcare) and eluted with the same borate buffer. The fractions containing DOTA-HSA were concentrated using concentrator columns (Pierce, 9K MWCO, 7mL) to a total volume of 500 μL. The purified DOTA-HSA was then reacted with 1 mg of Sulfo-SMCC in molar ratio of 1:5 and in a total volume of 200 μL for 1 h at 4 °C. The resulting bioconjugate was further purified using the PD-10 column and phosphate-buffered saline (PBS, pH 7.4) as the eluent. Finally, Ac-Cys-$Z_{HER2:342}$ was site specifically conjugated to the DOTA and Sulfo-SMCC modified HSA via the cysteine residue. The reaction was performed in a molar ratio of 1:5 using 200 μg of DOTA-HSA-SMCC and 150 μg of Ac-Cys-$Z_{HER2:342}$ in a total volume of 250 μL for 6 h at room temperature (Figure 2). The resulting bioconjugate, DOTA-HSA-$Z_{HER2:342}$, was then purified and concentrated through a microcentrifuge tube (Millipore, 30 kDa, 0.5 mL) to a final volume of 20 μL. After each step the protein concentration was measured by the bicinchoninic acid (BCA) assay (Pierce), and the samples were analyzed via MALDI-TOF-MS and sodium dodecyl sulfate polyacrylamide gel electrophoresis (SDS-PAGE).

Radiolabeling of DOTA-HSA-$Z_{HER2:342}$

Approximately 200 μg of the DOTA-HSA-$Z_{HER2:342}$ was radiolabeled with ^{64}Cu by addition of 37 MBq (1 mCi) of $^{64}CuCl_2$ in 0.1 N sodium acetate buffer (NaOAc, pH 6.0) and incubated for 1 h at 37 °C. For radiolabeling with ^{111}In, 74 MBq (2 mCi) of ^{111} $InCl_3$ in 0.1 N HCl was added to 150–200 μg of DOTA-HSA-$Z_{HER2:342}$ in ammonium acetate buffer (NH_4OAc, 0.25 M, pH 5.5), and the reaction proceeded for 90 min at 39 °C. The radiolabeled complex was purified by a PD-10column (GE Healthcare), eluted with PBS, and passed through a 0.22-μm Millipore filter for both *in vitro* cell uptake studies and animal experiments. Radiolabeling of DOTA-HSA with ^{64}Cu was performed in the same way as for DOTA-HSA-$Z_{HER2:342}$.

Cell Culture and In Vitro Cell Uptake Assays

The SKOV3 cells were cultured using the same protocol as previously reported (12). In vitro cell uptake assays of both ^{64}Cu-DOTA-HSA-$Z_{HER2:342}$ and ^{111}In-DOTA-HSA-$Z_{HER2:342}$ were performed as previously described with minor modifications (15). Briefly, SKOV3

cells (3×10^5) were seeded per well in 12-well tissue culture plates and allowed to attach overnight. Cells were washed twice with serum-free McCoy 5 medium and incubated with the probes [2 μCi per well, final concentration ~15 nM (0.5 μg)] in 400 μL of serum-free McCoy 5 medium at 37 °C.

The nonspecific binding of the probes with SKOV3 cells was determined by co-incubation with nonradioactive Ac-Cys-$Z_{HER2:342}$ (6 μg per well, final concentration 2.12 μM). After 0.5, 1 and 2 h the cells were washed three times with cold PBS and lysed in 200 μL of 0.2 M NaOH. The radioactivity of the cells was counted using a PerkinElmer 1470 automatic γ-counter. The uptake (counts/min) was expressed as the percentage of added radioactivity.

Small-Animal PET

All animal studies were performed in compliance with federal and local institutional rules for animal experimentation. Protocols were approved by the Stanford Administrative Panel on Laboratory Animal Care. Approximately 3×10^6 SKOV3 cells suspended in PBS were subcutaneously implanted in the right upper shoulders of female athymic nu/nu mice. Tumors were allowed to grow to a size of 0.5–0.7 cm in diameter (3–4 weeks). The tumor bearing mice were subjected to in vivo biodistribution and imaging studies. Small animal PET of tumor-bearing mice (n = 3 for each group) was performed using a micro-PET R4 rodent-model scanner (Siemens Medical Solutions USA, Inc.). Mice bearing SKOV3 tumors were injected with ^{64}Cu-DOTA-HSA-$Z_{HER2:342}$ (5.2–7.4 MBq, 140–200 μCi, 20–30 μg) via the tail vein. At various times after injection (1, 4, 24 and 48 h) the mice were anesthetized with 2% isoflurane and placed in the prone position and near the center of the field of view of the scanner. Static scans (for 1, 4 and 24 h, 3-min scans; for 48 h, 5-min scans) were obtained, and the images were reconstructed by a two-dimensional ordered subsets expectation maximum (OSEM) algorithm. As a control experiment mice bearing SKOV3 tumors were injected with^{64}Cu-DOTA-HSA (5.2–7.4 MBq, 140–200 μCi, 30–40 μg) via the tail vein. PET images were obtained in the same approach as for ^{64}Cu-DOTA-HSA-$Z_{HER2:342}$. The method for quantification analysis of small-animal PET images was the same as previously reported (13).

Small Animal SPECT/CT

For small animal single photon emission computed tomography and X-ray computed tomography (SPECT/CT), SKOV3 bearing mice (n = 3) were injected with ^{111}In-DOTA-HSA-$Z_{HER2:342}$ (14.8 MBq, 400–420 μCi, 80 μg) via the tail vein. After 24 h and 96 h, mice were anesthetized with 2% isoflurane and placed prone near the center of the field of view of the scanner. Radionuclide and CT imaging were performed on a combined SPECT/CT scanner for small animals (X-SPECT; Gamma Medica).

For micro-CT image acquisition, 512 images (170 μm slice thickness) were acquired in 5 minutes at 0.4 mA and 80 kVp. SPECT was performed using a 1 mm multi pinhole collimator (single head, 360° of rotation, 64 projections, 30 s/projection, and a 5 cm field-of-view). The SPECT images were then reconstructed by using an ordered subsets expectation-maximization (OSEM) algorithm with 8 subsets and 10 iterations into a 64 × 64 × 60 matrix size with a voxel size of 1.5 mm. CT images were reconstructed by using a cone-beam filtered backprojection algorithm into a 512 × 512 × 512 matrix with a voxel size of 170 μm. All data were imported into Amira (Mercury Computing Systems, Chelmsford) for processing and visualization.

Biodistribution Studies

For biodistribution studies, mice bearing SKOV3 xenografts (n = 3 for each group) were injected with 1.5–1.9 MBq (40–50 μCi, 5–10 μg) of ^{111}In-DOTA-HSA-$Z_{HER2:342}$ through

tail vein and sacrificed at different time points (1, 4, 24 and 48 h) post-injection (p.i.). To test the *HER2*–targeting specificity of ^{111}In-DOTA-HSA-$Z_{HER2:342}$ *in vivo*, SKOV3 tumor–bearing mice were injected with a mixture of the radiolabeled probe and 300 μg of unlabeled Ac-Cys-$Z_{HER2:342}$. Tumor and normal tissues were excised and weighed, and their radioactivity was measured using a γ-counter. The radioactivity uptake in the tumor and normal tissues was expressed as a % ID/g.

Radiation Absorbed Dose Calculation

Estimated radiation absorbed dose distribution in a human adult female was calculated using the biodistribution results on SKOV3 tumor bearing mice injected with ^{111}In-DOTA-HSA-$Z_{HER2:342}$ and OLINDA/EXM (RADAR, Vanderbilt University, Nashville, TN) software code based on the same % ID/organ (28–29). In brief, the cumulated activity in each organ (% ID × time) from 0 to 48 h was obtained by calculating the area under the % ID – time curve. Blood activity at time 0 was obtained by extrapolating the simulated exponential decay curve of radioactivity in the blood from 1 to 48 h. Radioactivity in other organs at time 0 was assumed as 0 and it was also assumed a linear accumulation of radioactivity in other organs from time 0 to 1 h. Percent ID in each organ was decay corrected before the use for cumulated activity calculation. The number of disintegrations in each major organ (cumulated activity in % ID × time)/100 was then input into OLINDA/EXM software for radiation absorbed dose calculation. To calculate radiation absorbed doses in ovarian cancer, ovary organ was assumed as a tumor with a weight of 11 g in the radiation absorbed dose calculation model.

Statistical Analysis

Statistical analysis was performed using Student's two-tailed *t*-test for unpaired data. A 95% confidence level was chosen to determine the significance between groups, with $P < 0.05$ being significantly different.

RESULTS

Conjugation Chemistry and Radiochemistry

Ac-Cys-$Z_{HER2:342}$ with a cysteine residue at the N-terminal was successfully synthesized through conventional solid phase peptide synthesis and purified by a semi-preparative HPLC as described for the Ac-Cys-$Z_{EGFR:1907}$ (27). The purity of Ac-Cys-$Z_{HER2:342}$ was > 95% and the retention time on analytical C4 HPLC for Ac-Cys-$Z_{HER2:342}$ was found to be 18 min. The measured molecular weight (MW) of the purified Ac-Cys-$Z_{HER2:342}$ was consistent with the expected MW: *m/z* = 6847.6 for $[M+H]^+$ (calculated MW $[M+H]^+$ = 6850.7) as characterized by MALDI-TOF-MS. The N-terminal cysteine residue in the engineered anti-*HER2* Affibody molecule provides a thiol moiety that can be used for site-specific coupling to HSA proteins.

The molecular weights of HSA-DOTA and HSA-DOTA coupled with bifunctional linker SMCC (DOTA-HSA-SMCC) were found to be *m/z* = 67.46 kDa and *m/z* = 68.56 kDa, respectively. When compared to HSA (*m/z* = 66.48 kDa), about two DOTA molecules and 6–7 maleimide groups are coupled to one HSA molecule. For the conjugation of DOTA-HSA-SMCC with Ac-Cys-$Z_{HER2:342}$, MALDI-TOF-MS showed one peak corresponding to unreacted DOTA-HSA-SMCC (a) and another five peaks with MW of 75.03 (b), 82.09 (c), 89.19 (d), 95.8 (e) and 102.19 (f) kDa (Figure 3A), which represent different numbers of Affibody molecules (1 to 5) on a HSA protein. This result was also confirmed by SDS-PAGE analysis which shows a broad band of the DOTA-HSA-$Z_{HER2:342}$ caused by different numbers of Affibody molecules linked to HSA (Figure 3B). The Ac-Cys-$Z_{HER2:342}$ was

completely removed from the final DOTA-HSA-$Z_{HER2:342}$ bioconjugates as demonstrated by SDS-PAGE analysis.

DOTA-HSA-$Z_{HER2:342}$ was then successfully radiolabeled with either ^{64}Cu or ^{111}In. Purification of the radioactive reaction mixtures using a PD-10 column resulted in ^{64}Cu-DOTA-HSA-$Z_{HER2:342}$ and ^{111}In-DOTA-HSA-$Z_{HER2:342}$ with a decay-corrected yield of more than 80% and around 60%, respectively. High specific activities of 12–14 MBq of ^{64}Cu-DOTA-HSA-$Z_{HER2:342}$ per nanomole (4.3–5.0 mCi/mg) and 14–33 MBq of ^{111}In-DOTA-HSA-$Z_{HER2:342}$ per nanomole (5.0–11.9 mCi/mg) were obtained at the end of synthesis.

In Vitro Cell Uptake Assays

Cell uptakes of ^{64}Cu-DOTA-HSA-$Z_{HER2:342}$ and ^{111}In-DOTA-HSA-$Z_{HER2:342}$ at 37 °C over incubation periods of 0.5, 1 and 2 h are shown in Figure 4A and B, respectively. ^{64}Cu-DOTA-HSA-$Z_{HER2:342}$ slowly accumulated in the SKOV3 cells and reached 0.71 ± 0.05% of the applied activity at 0.5 h. The uptake increased to 1.58 ± 0.09% at 2 h (Figure 4A). A similar cell uptake pattern was observed for ^{111}In-DOTA-HSA-$Z_{HER2:342}$. The uptake increased from 0.85 ± 0.15% at 0.5 h up to 1.46 ± 0.2% at 2 h. When incubated with a large excess of Ac-Cys-$Z_{HER2:342}$, SKOV3 cells showed significantly inhibited uptakes of both probes ($P < 0.05$) at all incubation time points. These results clearly demonstrate specific *HER2* receptor binding abilities of both probes.

Small Animal PET

Decay-corrected coronal microPET images of a mouse bearing SKOV3 tumor at 1, 4, 24 and 48 h after tail vein injection of ^{64}Cu-DOTA-HSA-$Z_{HER2:342}$ and ^{64}Cu-DOTA-HSA are shown in Figure 5A and B, respectively. For ^{64}Cu-DOTA-HSA-$Z_{HER2:342}$, the SKOV3 tumor was visible with a low tumor-to-background contrast at 1 h p.i., but with a very good tumor-to-background contrast at 4 and 24 h p.i. The tumor was still clearly visualized at 48 h p.i. Quantification analysis revealed that the SKOV3 tumor uptake values increased with time and were found to be 5.63 ± 2.07, 9.98 ± 2.66, 14.34 ± 3.22 and 14.12 ± 2.22% ID/g at 1, 4, 24, and 48 h, respectively (Figure 5C). In addition to the tumor, high activity accumulations were also observed in the liver (12.92 ± 2.4% ID/g at 24 h), but much lower activity accumulations in the kidneys (4.17 ± 1.01% ID/g at 24 h). Furthermore, relatively high radioactivity concentrations were found in the blood (ROI over the heart) with 22.04 ± 1.79 and 13.95 ± 1.62 at 1 h and 4 h p.i., respectively (Figure 5D). For comparison, ^{64}Cu-DOTA-HSA showed similar distribution patterns as for ^{64}Cu-DOTA-HSA-$Z_{HER2:342}$ in most normal organs except for the tumor (Figure 5A and B). About a 2 to 3-fold higher tumor uptake ($P < 0.05$) was observed for ^{64}Cu-DOTA-HSA-$Z_{HER2:342}$ compared to the ^{64}Cu-DOTA-HSA at 4 h, 24 h and 48 h(Figure 5C).

Small Animal SPECT/CT

SPECT/CT confirmed high tumor targeting properties of ^{111}In-DOTA-HSA-$Z_{HER2:342}$ in SKOV3 tumor-bearing mice (Figure 6). Images acquired at 24 h and 96 h after injection demonstrated a significant tumor localization and high tumor to background contrasts. High radioactivity accumulation in the liver while much lower uptake in the kidneys indicated the hepatobiliar route of elimination of the ^{111}In-DOTA-HSA-$Z_{HER2:342}$.

Biodistribution Studies

The *in vivo* biodistribution of ^{111}In-DOTA-HSA-$Z_{HER2:342}$ was examined in a SKOV3 human ovarian tumor-bearing mouse model. The biodistribution of the ^{111}In-DOTA-HSA-$Z_{HER2:342}$ at 1 h, 4 h, 24 h and 48 h are shown in Table 1. Slow but high levels of

radioactivity accumulation in the SKOV3 tumors were observed. The tumor uptake in SKOV3 tumors measured was 4.61% ID/g at 1 h and continually increased to 12.52% ID/g at 4 h and then reached a plateau of 16.26 and 16.73% ID/g at 24 hand 48 h, respectively (Table 1). The ^{111}In-DOTA-HSA-$Z_{HER2:342}$ also displayed relatively slow blood clearance. Blood values of 25.95% ID/g and 20.11% ID/g were observed at 1 h and 4 h after injection, respectively. Furthermore, the probe displayed high levels of liver uptake at all time points (e.g., 4 h after injection; more than 15% ID/g). The kidneys, however, showed a moderate radioactivity accumulation (e.g., 9.95% ID/g and 6.06% ID/g at 4 h and 24 h after injection, respectively). This data suggests that the probe was cleared predominantly through the hepatobiliary system and to a minor part through the renal system. The *in vivo* tumor-targeting specificity was further proved by co-injection of the non-radioactive Ac-Cys-$Z_{HER2:342}$. Compared to non-treated groups, co-injection of large excess of Affibody protein could significantly reduce the SKOV3 tumor uptake to around 51% of the corresponding uptake at 4 h p.i. (12.52% ID/g *vs.* 6.49% ID/g, $P < 0.01$). Consequently, the tumor-to-muscle ratio was significantly decreased for the blocking group (11.12 *vs.* 4.2, $P < 0.01$).

Radiation Dosimetry

Estimated human absorbed doses to normal organs for ^{111}In-DOTA-HSA-$Z_{HER2:342}$ were presented in Figure 7. The results predict that the highest radiation-absorbed doses will be in the tumor (3.43 mGy/MBq), and the whole-body absorbed dose was found to be 0.032 mGy/MBq. Among the other normal organs, liver (0.23 mGy/MBq), kidney (0.17 mGy/MBq) and spleen (0.13 mGy/MBq) show the highest radiation-absorbed doses. It should be noted that these dose estimations for humans are extrapolated from murine data and thus the numbers may not correlate exactly with the actual dose distribution results in patients. The real patient specific dosimetry still needs to be performed in patient studies.

DISCUSSION

In preclinical studies, Affibody scaffolds have shown promising prospects in numerous *HER2*-specific targeting applications. Moreover, the recent first application of ^{68}Ga- and ^{111}In-labeled DOTA-$Z_{HER2:342\text{-}pep2}$ (ABY-002) in patients with metastatic breast cancer highlights the great potential of Affibody molecules to localize themselves to *HER2*-positive metastatic lesions in patients (30). However, the use of Affibody molecules for radiotherapeutic applications is questionable, mainly due to their relatively fast clearance (compared to antibody) and extremely high kidney uptakes (generally > 100% ID/g for radiometal-labeled Affibody scaffolds) (8,15–16). The high renal accumulation of the radiometal-labeled Affibody molecules could result in very high radiation doses to the radiation-sensitive kidneys. Therefore this represents a critical concern for using Affibody molecules for radionuclide therapy. Thus, we aimed to develop a generalizable strategy to design Affibody bioconjugates which possess high tumor targeting specificity as well as low kidney accumulations.

As shown in earlier studies, the fusion of an Affibody protein to a small albumin binding domain (ABD) results in a 20 kDa Affibody-ABD fusion protein that shows reduced kidney uptake and that can be efficient in radionuclide therapy approaches (31–32). Inspired by these results, we explored a simple and generalizable method to chemically conjugate several Affibody molecules to HSA for *in vivo* applications. The resulting bioconjugate is a multimeric ligand with a size much below conventional antibodies (< 100 kDa). The chemical conjugation of Affibody molecules to HSA has several distinctive advantages compared to Affibody-ABD fusion proteins. First, our method avoids time-consuming techniques, such as molecular cloning and protein purification. Moreover, compared to the Affibody-ABD fusion proteins, the conjugation used in this paper is more versatile, and allows for a quick and efficient conjugation of many other peptides or proteins in a similar

fashion. Second, the HSA modification not only improves the pharmacokinetics of the Affibody (e.g. reduced kidney uptake) due to a higher molecular weight, it also allows the attachment of multiple monomeric ligands to one HSA molecule. This may allow multiple and simultaneous binding to *HER2* receptors and lead to an improved tumor targeting efficacy and retention. The advantages of using multivalent binders have been well documented and reviewed before (33–34). Third, covalent conjugation of the Affibody molecule to HSA seems to be a more accessible approach than a non-covalent binding of the Affibody-fusion protein to the patients' own serum albumin *in vivo*.

The synthesis of chemically conjugated DOTA-HSA-$Z_{HER2:342}$ was performed in three steps. First, HSA was modified with the metal chelator DOTA. It was found that two DOTA were coupled with one HSA molecule. The conjugation of DOTA to the backbone of HSA as the first step is advantageous and avoids a potential unfavorable modification of the Affibody protein. On the contrary, for radiolabeling of many Affibody proteins or preparations of Affibody-ABD fusion proteins, the lysine residues in the Affibody molecules were used for sites of chemical modification (6,8,31–32). These approaches are not ideal and may generate products with reduced targeting capacity because multiple lysine residues presented in the Affibody are responsible for receptor recognition. Second, the bifunctional crosslinker Sulfo-SMCC was conjugated to DOTA-HSA through lysine residues. As shown by MALDI-TOF-MS analyses, 6 to 8 reactive groups were found on one HSA molecule. In the third step, the *HER2*Affibody analog Ac-Cys-$Z_{HER2:342}$ was covalently conjugated with DOTA-HSA-SMCC. It was found that up to five Affibody molecules were covalently conjugated onto one HSA molecule. We also tested different Affibody-to-HSA reaction ratios and found that higher ratios of Affibody molecules did not result in a higher number of attached Affibody molecules (data not shown).

Evaluation of the radiolabeled conjugates in mice demonstrated that ^{64}Cu-DOTA-HSA-$Z_{HER2:342}$ and ^{111}In-DOTA-HSA-$Z_{HER2:342}$ are promising agents for *HER2* imaging via PET and SPECT/CT. For small-animal PET, excellent tumor-to- background contrast was obtained at 4 h, 24 h, and 48 h after injection of ^{64}Cu-DOTA-HSA-$Z_{HER2:342}$.Whereas the SKOV3 tumors in ^{64}Cu-DOTA-HSA injected mice could be barely seen. Quantitative analysis of PET images suggested a significant difference in tumor uptake of ^{64}Cu-DOTA-HSA-$Z_{HER2:342}$ and ^{64}Cu-DOTA-HSA. This is a good reflection of the specificity of ^{64}Cu-DOTA-HSA-$Z_{HER2:342}$ in *HER2* positive tumors. Micro SPECT/CT with ^{111}In-DOTA-HSA-$Z_{HER2:342}$ clearly showed uptake into the tumors of mice at 24 h p.i. and even at 96 h p.i. For both PET and SPECT imaging the kidneys showed low uptakes. These imaging studies clearly indicate that HSA modification does not compromise the tumor targeting ability of the Affibody molecules, while significantly reducing the kidney uptakes of the protein.

The biodistribution studies of ^{111}In-DOTA-HSA-$Z_{HER2:342}$ showed the capacity of ^{111}In-DOTA-HSA-$Z_{HER2:342}$ to accumulate in HER2 expressing tumors. Such findings were in good agreement with the PET studies of ^{64}Cu-DOTA-HSA-$Z_{HER2:342}$ in xenograft-bearing mice. Due to the relatively high molecular weight of the compound (~ 75.4 to 96.2 kDa), the probe exhibited mainly a hepatic accumulation.

Additionally, spleen uptake was found to be high probably due to uptake through scavenger receptors in sessile macrophages within the spleen. Consistent with our expectation, the kidney retention (11.50% ID/g at 1 h and 5.37% ID/g at 48 h) of the conjugate was very low in comparison to the radiometal-labeled Affibody monomer itself (16,19), trastuzumab (35–36), anti-HER2 diabodies (37) or minibodies (38). Furthermore, the reduction of the renal clearance could be decreased to even lower levels compared to an ^{177}Lu-labelled Affibody-ABD fusion protein (15% *vs* 6.1% ID/g) as shown in biodistribution experiments in SKOV3

tumor bearing mice (31). The specificities of ^{111}In-DOTA-HSA-Z$_{HER2:342}$ were also confirmed by the use of an excess of nonradiolabeled Ac-Cys-Z$_{HER2:342}$ *in vitro* and *in vivo*. Biodistribution studies revealed a specific binding of ^{111}In-DOTA-HSA-Z$_{HER2:342}$ to *HER2* protein as shown by a reduced SKOV3 tumor uptake after co-injection with Ac-Cys-Z $_{HER2:342}$.

CONCLUSION

DOTA-HSA-Z$_{HER2:342}$ bioconjugates were successfully chemically synthesized and labeled with radiometals. These probes provide high specificity, sensitivity, and display excellent tumor contrasts as shown in PET and SPECT studies. This exemplifies their potential for the imaging of *HER2* positive cancer. More importantly, the *in vivo* properties and pharmacokinetics of DOTA-HSA-Z$_{HER2:342}$ conjugates make them promising candidates for labeling with therapeutic radionuclides, e.g. ^{90}Y or ^{177} Lu.

This proof of concept research of using HSA to alternate the pharmacokinetic and biodistribution of biomolecules such as Affibody molecules indicates a broader application towards many other imaging and radionuclide therapy agents.

Acknowledgments

This work was supported, in part, by National Cancer Institute (NCI) 5R01 CA119053 and NCI in Vivo Cellular Molecular Imaging Center (ICMIC) grant P50 CA114747. The authors thank Dr. Timothy Doyle for his expert knowledge and technical advice in SPECT-CT imaging.

References

1. Slamon DJ, Godolphin W, Jones LA, Holt JA, Wong SG, Keith DE, Levin WJ, Stuart SG, Udove J, Ullrich A, et al. Studies of the HER-2/neu proto-oncogene in human breast and ovarian cancer. Science. 1989; 244:707–12. [PubMed: 2470152]
2. Schneider PM, Hung MC, Chiocca SM, Manning J, Zhao XY, Fang K, Roth JA. Differential expression of the c-erbB-2 gene in human small cell and non-small cell lung cancer. Cancer Res. 1989; 49:4968–71. [PubMed: 2569928]
3. Yokota J, Yamamoto T, Miyajima N, Toyoshima K, Nomura N, Sakamoto H, Yoshida T, Terada M, Sugimura T. Genetic alterations of the c-erbB-2 oncogene occur frequently in tubular adenocarcinoma of the stomach and are often accompanied by amplification of the v-erbA homologue. Oncogene. 1988; 2:283–7. [PubMed: 3281095]
4. Nilsson FY, Tolmachev V. Affibody molecules: new protein domains for molecular imaging and targeted tumor therapy. Curr Opin Drug Discov Devel. 2007; 10:167–75.
5. Nord K, Gunneriusson E, Ringdahl J, Stahl S, Uhlen M, Nygren PA. Binding proteins selected from combinatorial libraries of an alpha-helical bacterial receptor domain. Nat Biotechnol. 1997; 15:772–7. [PubMed: 9255793]
6. Orlova A, Magnusson M, Eriksson TL, Nilsson M, Larsson B, Hoiden-Guthenberg I, Widstrom C, Carlsson J, Tolmachev V, Stahl S, Nilsson FY. Tumor imaging using a picomolar affinity HER2 binding affibody molecule. Cancer Res. 2006; 66:4339–48. [PubMed: 16618759]
7. Wikman M, Steffen AC, Gunneriusson E, Tolmachev V, Adams GP, Carlsson J, Stahl S. Selection and characterization of HER2/neu-binding affibody ligands. Protein Eng Des Sel. 2004; 17:455–62. [PubMed: 15208403]
8. Tolmachev V, Nilsson FY, Widstrom C, Andersson K, Rosik D, Gedda L, Wennborg A, Orlova A. 111In-benzyl-DTPA-ZHER2:342, an affibody-based conjugate for in vivo imaging of HER2 expression in malignant tumors. J Nucl Med. 2006; 47:846–53. [PubMed: 16644755]
9. Kramer-Marek G, Kiesewetter DO, Martiniova L, Jagoda E, Lee SB, Capala J. [18F]FBEM-Z(HER2:342)-Affibody molecule-a new molecular tracer for in vivo monitoring of HER2 expression by positron emission tomography. Eur J Nucl Med Mol Imaging. 2008; 35:1008–18. [PubMed: 18157531]

10. Tran T, Engfeldt T, Orlova A, Sandstrom M, Feldwisch J, Abrahmsen L, Wennborg A, Tolmachev V, Karlstrom AE. (99m)Tc-maEEE-Z(HER2:342), an Affibody molecule-based tracer for the detection of HER2 expression in malignant tumors. Bioconjug Chem. 2007; 18:1956–64. [PubMed: 17944527]
11. Steffen AC, Almqvist Y, Chyan MK, Lundqvist H, Tolmachev V, Wilbur DS, Carlsson J. Biodistribution of 211At labeled HER-2 binding affibody molecules in mice. Oncol Rep. 2007; 17:1141–7. [PubMed: 17390057]
12. Fortin MA, Orlova A, Malmstrom PU, Tolmachev V. Labelling chemistry and characterization of [90Y/177Lu]-DOTA-ZHER2:342–3 Affibody molecule, a candidate agent for locoregional treatment of urinary bladder carcinoma. Int J Mol Med. 2007; 19:285–91. [PubMed: 17203203]
13. Cheng Z, De Jesus OP, Namavari M, De A, Levi J, Webster JM, Zhang R, Lee B, Syud FA, Gambhir SS. Small-animal PET imaging of human epidermal growth factor receptor type 2 expression with site-specific 18F-labeled protein scaffold molecules. J Nucl Med. 2008; 49:804–13. [PubMed: 18413392]
14. Lee SB, Hassan M, Fisher R, Chertov O, Chernomordik V, Kramer-Marek G, Gandjbakhche A, Capala J. Affibody molecules for in vivo characterization of HER2-positive tumors by near-infrared imaging. Clin Cancer Res. 2008; 14:3840–9. [PubMed: 18559604]
15. Ren G, Zhang R, Liu Z, Webster JM, Miao Z, Gambhir SS, Syud FA, Cheng Z. A 2-helix small protein labeled with 68Ga for PET imaging of HER2 expression. J Nucl Med. 2009; 50:1492–9. [PubMed: 19690041]
16. Cheng Z, De Jesus OP, Kramer DJ, De A, Webster JM, Gheysens O, Levi J, Namavari M, Wang S, Park JM, Zhang R, Liu H, Lee B, Syud FA, Gambhir SS. 64Cu-labeled affibody molecules for imaging of HER2 expressing tumors. Mol Imaging Biol. 2010; 12:316–24. [PubMed: 19779897]
17. Engfeldt T, Orlova A, Tran T, Bruskin A, Widstrom C, Karlstrom AE, Tolmachev V. Imaging of HER2-expressing tumours using a synthetic Affibody molecule containing the 99mTc-chelating mercaptoacetyl-glycyl-glycyl-glycyl (MAG3) sequence. Eur J Nucl Med Mol Imaging. 2007; 34:722–33. [PubMed: 17146656]
18. Engfeldt T, Tran T, Orlova A, Widstrom C, Feldwisch J, Abrahmsen L, Wennborg A, Karlstrom AE, Tolmachev V. 99mTc- chelator engineering to improve tumour targeting properties of a HER2-specific Affibody molecule. Eur J Nucl Med Mol Imaging. 2007; 34:1843–53. [PubMed: 17565496]
19. Orlova A, Rosik D, Sandstrom M, Lundqvist H, Einarsson L, Tolmachev V. Evaluation of [(111/114m)In]CHX-A″-DTPA- ZHER2:342, an affibody ligand coniugate for targeting of HER2-expressing malignant tumors. Q J Nucl Med Mol Imaging. 2007; 51:314–23. [PubMed: 17464277]
20. Orlova A, Tolmachev V, Pehrson R, Lindborg M, Tran T, Sandstrom M, Nilsson FY, Wennborg A, Abrahmsen L, Feldwisch J. Synthetic affibody molecules: a novel class of affinity ligands for molecular imaging of HER2-expressing malignant tumors. Cancer Res. 2007; 67:2178–86. [PubMed: 17332348]
21. Orlova A, Tran T, Widstrom C, Engfeldt T, Eriksson Karlstrom A, Tolmachev V. Pre-clinical evaluation of [111In]-benzyl-DOTA-Z(HER2:342), a potential agent for imaging of HER2 expression in malignant tumors. Int J Mol Med. 2007; 20:397–404. [PubMed: 17671747]
22. Tolmachev V, Velikyan I, Sandstrom M, Orlova A. A HER2-binding Affibody molecule labelled with (68)Ga for PET imaging: direct in vivo comparison with the (111)In-labelled analogue. Eur J Nucl Med Mol Imaging. 2010
23. Tran T, Orlova A, Sivaev I, Sandstrom M, Tolmachev V. Comparison of benzoate- and dodecaborate-based linkers for attachment of radioiodine to HER2-targeting Affibody ligand. Int J Mol Med. 2007; 19:485–93. [PubMed: 17273798]
24. Tran TA, Ekblad T, Orlova A, Sandstrom M, Feldwisch J, Wennborg A, Abrahmsen L, Tolmachev V, Eriksson Karlstrom A. Effects of lysine-containing mercaptoacetyl-based chelators on the biodistribution of 99mTc-labeled anti-HER2 Affibody molecules. Bioconjug Chem. 2008; 19:2568–76. [PubMed: 19035668]
25. Gradishar WJ. Albumin-bound paclitaxel: a next-generation taxane. Expert Opin Pharmacother. 2006; 7:1041–53. [PubMed: 16722814]

26. Chen K, Xie J, Chen X. RGD-human serum albumin conjugates as efficient tumor targeting probes. Mol Imaging. 2009; 8:65–73. [PubMed: 19397852]
27. Miao Z, Ren G, Liu H, Jiang L, Cheng Z. Small-animal PET imaging of human epidermal growth factor receptor positive tumor with a 64Cu labeled affibody protein. Bioconjug Chem. 2010; 21:947–54. [PubMed: 20402512]
28. Stabin MG, Sparks RB, Crowe E. OLINDA/EXM: the second-generation personal computer software for internal dose assessment in nuclear medicine. J Nucl Med. 2005; 46:1023–7. [PubMed: 15937315]
29. Eckerman, KF.; Endo, A. MIRD: Radionuclide Data and Decay Schemes. Society of Nuclear Medicine; Reston: 2008.
30. Baum RP, Prasad V, Muller D, Schuchardt C, Orlova A, Wennborg A, Tolmachev V, Feldwisch J. Molecular imaging of HER2-expressing malignant tumors in breast cancer patients using synthetic 111In- or 68Ga-labeled affibody molecules. J Nucl Med. 2010; 51:892–7. [PubMed: 20484419]
31. Tolmachev V, Orlova A, Pehrson R, Galli J, Baastrup B, Andersson K, Sandstrom M, Rosik D, Carlsson J, Lundqvist H, Wennborg A, Nilsson FY. Radionuclide therapy of HER2-positive microxenografts using a 177Lu-labeled HER2-specific Affibody molecule. Cancer Res. 2007; 67:2773–82. [PubMed: 17363599]
32. Tolmachev V, Wallberg H, Andersson K, Wennborg A, Lundqvist H, Orlova A. The influence of Bz-DOTA and CHX-A″-DTPA on the biodistribution of ABD-fused anti-HER2 Affibody molecules: implications for (114m)In-mediated targeting therapy. Eur J Nucl Med Mol Imaging. 2009; 36:1460–8. [PubMed: 19430786]
33. Liu S. Radiolabeled multimeric cyclic RGD peptides as integrin alphavbeta3 targeted radiotracers for tumor imaging. Mol Pharm. 2006; 3:472–87. [PubMed: 17009846]
34. Liu S. Radiolabeled cyclic RGD peptides as integrin alpha(v)beta(3)-targeted radiotracers: maximizing binding affinity via bivalency. Bioconjug Chem. 2009; 20:2199–213. [PubMed: 19719118]
35. Tang Y, Wang J, Scollard DA, Mondal H, Holloway C, Kahn HJ, Reilly RM. Imaging of HER2/neu-positive BT-474 human breast cancer xenografts in athymic mice using (111)In-trastuzumab (Herceptin) Fab fragments. Nucl Med Biol. 2005; 32:51–8. [PubMed: 15691661]
36. Smith-Jones PM, Solit DB, Akhurst T, Afroze F, Rosen N, Larson SM. Imaging the pharmacodynamics of HER2 degradation in response to Hsp90 inhibitors. Nat Biotechnol. 2004; 22:701–6. [PubMed: 15133471]
37. Adams GP, Shaller CC, Dadachova E, Simmons HH, Horak EM, Tesfaye A, Klein-Szanto AJ, Marks JD, Brechbiel MW, Weiner LM. A single treatment of yttrium-90-labeled CHX-A″-C6.5 diabody inhibits the growth of established human tumor xenografts in immunodeficient mice. Cancer Res. 2004; 64:6200–6. [PubMed: 15342405]
38. Olafsen T, Tan GJ, Cheung CW, Yazaki PJ, Park JM, Shively JE, Williams LE, Raubitschek AA, Press MF, Wu AM. Characterization of engineered anti-p185HER-2 (scFv-CH3)2 antibody fragments (minibodies) for tumor targeting. Protein Eng Des Sel. 2004; 17:315–23. [PubMed: 15187222]

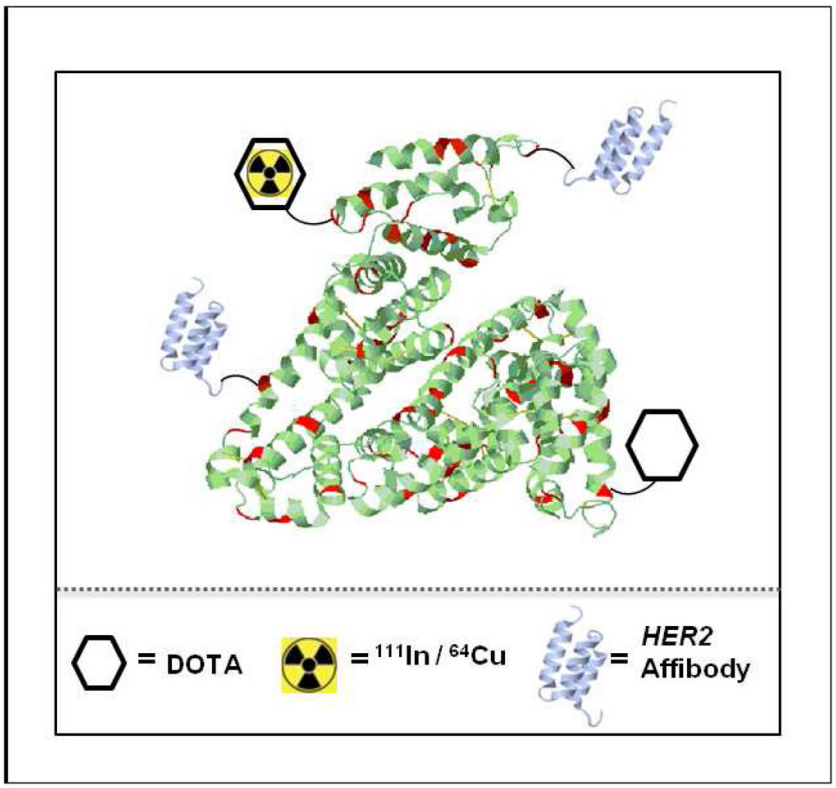

FIGURE 1.

Schematic structure of a radiolabeled Affibody-HSA conjugate. Red regions indicate the lysine residues of HSA suitable for the conjugation with DOTA (hexagon) and HER2-Affibody molecules (violet structures). The yellow symbols indicate the radiometals 111In and 64Cu, respectively. 108×101mm (150 × 150 DPI)

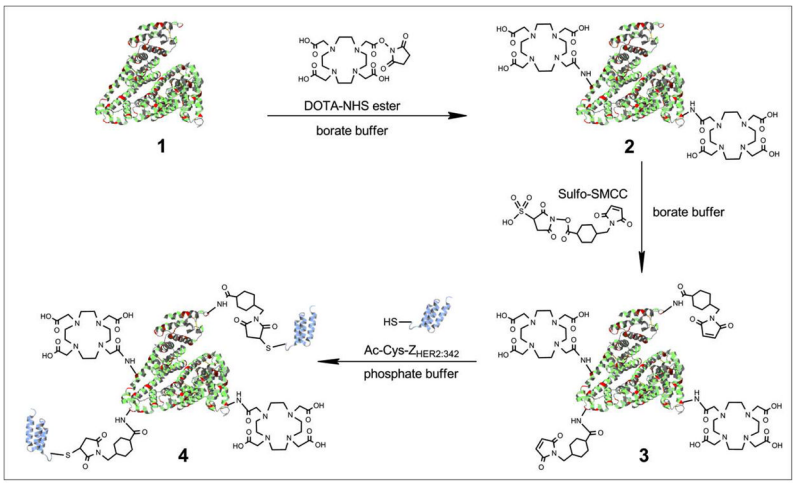

FIGURE 2.

Synthetic schemes for the chemical conjugation of DOTA, ZHER2:342 and HSA. (1) HSA, the red regions indicate the lysine residues; (2) HSA conjugated with DOTA-NHS to produce DOTA-HSA; (3) DOTA-HSA conjugated with the bifunctional crosslinker Sulfo-SMCC to generate DOTA-HSA-SMCC; (4) Chemically conjugated ZHER2:342 (violet structure) with DOTA-HSA-SMCC to obtain the final product DOTA-HSA-ZHER2:342. 258×154mm (150 × 150 DPI)

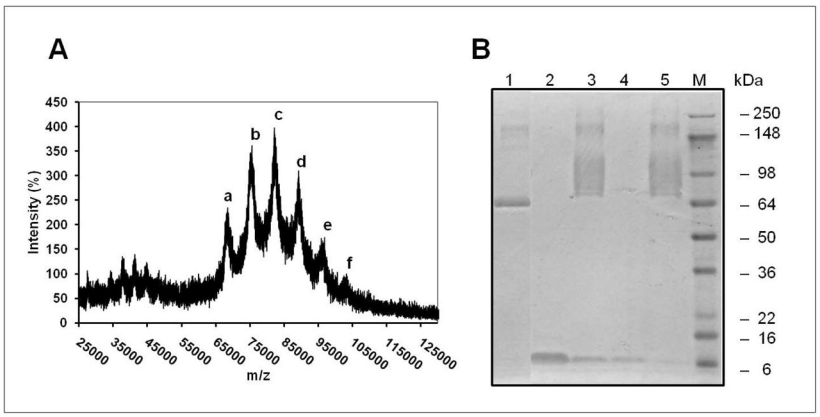

FIGURE 3.

Analysis of Affibody-HSA bioconjugates. (A) MALDI-TOF-MS of DOTA-HSA-ZHER2:342. The number of Affibody molecules per HSA is calculated to be 1 to 5. (a), DOTA-HSA-SMCC 68.56 kDa; (b), DOTA-HSA-ZHER2:342(1) (MW=75.03); (c), DOTA-HSA-ZHER2:342(2) (MW=82.09); (d), DOTA-HSA-ZHER2:342(3) (MW= 89.19); (e), DOTA-HSA-ZHER2:342(4) (95.8 kDa) and (f), DOTA-HSA-ZHER2:342(5) (MW= 102.19) (B) SDS-PAGE analysis of several fractions obtained from the chemical conjugation procedure of HSA with ZHER2:342. 1, HSA; 2, Ac-Cys-ZHER2:342; 3, reaction mixture of DOTA-HSA and ZHER2:342 (DOTA-HSA-ZHER2:342); 4, flow-through fraction after centrifugation using microcentrifuge tubes; 5, purified DOTA-HSA-ZHER2:342. 241×120mm (150 × 150 DPI)

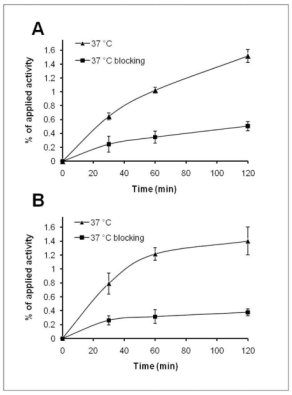

FIGURE 4.

Uptake of 64Cu-DOTA-HSA-ZHER2:342 (A) and 111In-DOTA-HSA-ZHER2:342 (B) in SKOV3 cells over time at 37 °C in presence or absence of non-radioactive Ac-Cys-ZHER2:342. All results are expressed as percentage of applied radioactivity and are mean of six measurements ± SD. 133×180mm (150 × 150 DPI)

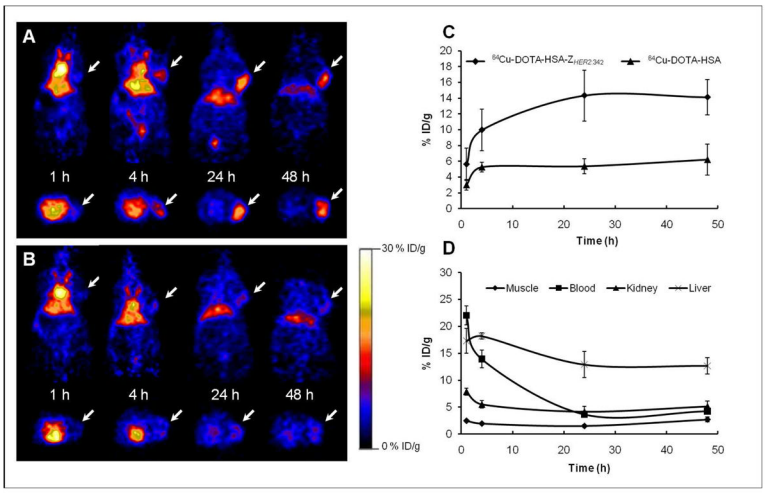

FIGURE 5.

Micro-PET imaging in nude mice bearing SKOV3 tumors. Representative decay corrected coronal (top) and transaxial (bottom) PET images at 1 h, 4 h, 24 h and 48 h after tail vein injection of 64Cu-DOTA-HSA-ZHER2:342 (A) and of 64Cu-DOTA-HSA as control (B). Arrows indicate the location of tumors. (C) Tumor time-activity curves derived from multiple-time-point small-animal PET images after tail vein injection of 64Cu-DOTA-HSA-ZHER2:342 and of 64Cu-DOTA-HSA. (D) Time–activity curves of muscle, blood, liver and kidney derived from multiple-time-point small-animal PET images after tail vein injection of 64Cu-DOTA-HSA-ZHER2:342. Data presented in (C) and (D) are shown as mean ± SD % ID/g (n = 3). 290×184mm (150 × 150 DPI)

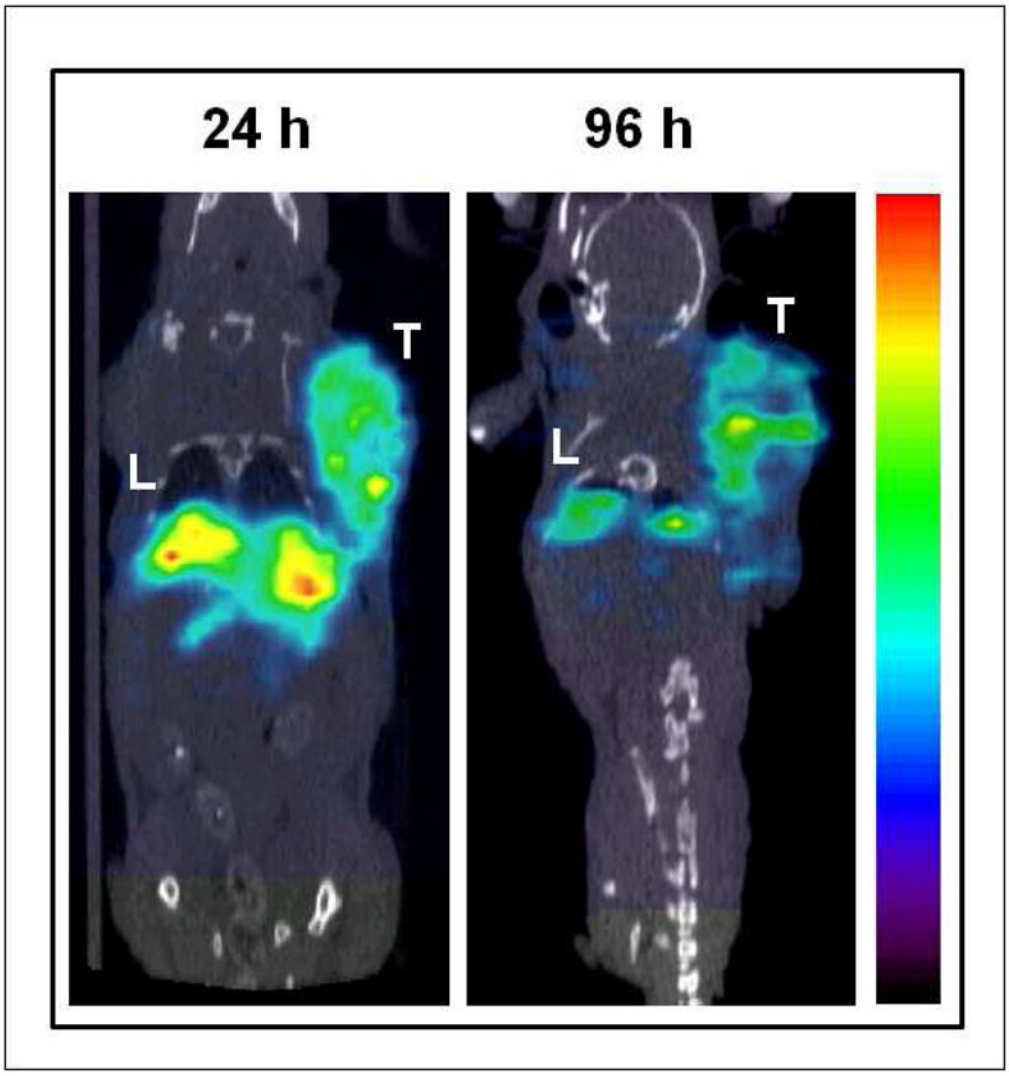

FIGURE 6.
Small Animal SPECT/CT of a mouse bearing SKOV3 tumor xenograft at 24 h and 96 h after administration of 111In-DOTA-HSA-ZHER2:342. T, tumor; L, liver. Red color indicates highest radioactivity concentration. 99×106mm (150 × 150 DPI)

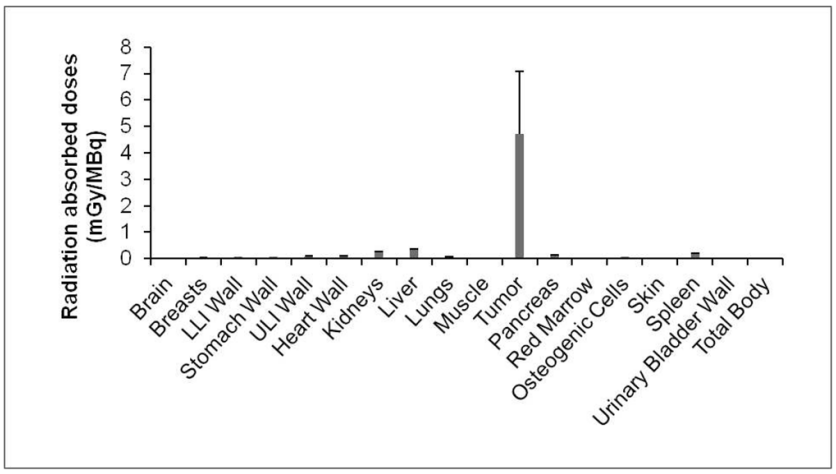

FIGURE 7.

Estimated radiation absorbed doses in major organs of a human adult male after intravenous injection of 111In-DOTA-HSA-ZHER2:342 based on the biodistribution data obtained in SKOV3-tumor bearing mice. Abbreviations: LLI, lower large intestine; ULI: upper large intestine. 163×91mm (150 × 150 DPI)

TABLE 1

Biodistribution results for ^{111}In-DOTA-HSA-Z$_{HER2:342}$ in nude mice bearing subcutaneously xeno-transplanted SKOV3 human ovarian cancer. Data are expressed as the percentage administered activity (injected dose) per gram of tissue (% ID/g) after intravenous injection of the probe at 1, 4, 24 and 48 h (n = 3). For 4 h-block, mice were co-injected with the radioactive probe and 300 μg of Ac-Cys-Z$_{HER2:342}$.

Site	1 h	4 h	4h - block	24 h	48 h
Blood	25.95 ± 3.54	20.11 ± 3.5	19.43 ± 1.51	5.15 ± 0.68	3.02 ± 0.87
Tumor	4.61 ± 0.46	12.52 ± 1.13*	6.49 ± 0.59	16.26 ± 1.33	16.73 ± 1.16
Heart	9.05 ± 3.13	8.18 ± 0.90	7.88 ± 0.37	2.19 ± 1.5	3.37 ± 0.5
Liver	11.79 ± 2.89	15.56 ± 1.84	18.41 ± 1.53	14.11 ± 2.61	13.56 ± 2.94
Lungs	11.54 ± 3.37	11.64 ± 2.68	10.68 ± 0.92	3.5 ± 0.46	2.56 ± 0.61
Muscle	1.09 ± 0.67	1.14 ± 0.19	1.67 ± 0.48	1.15 ± 0.54	1.04 ± 0.27
Spleen	7.66 ±1.5	10.24 ± 0.42	9.69 ± 0.61	7.08 ± 0.68	8.71 ± 1.12
Skin	1.86 ± 0.89	4.11 ± 1.65	3.99 ± 1.19	5.99 ± 0.06	5.2 ± 0.73
Bone	3.58 ± 0.72	3.49 ± 1.27	2.99 ± 0.22	2.9 ± 0.28	3.33 ± 0.05
Kidneys	11.5 ± 2.05	9.95 ± 0.67*	8.11 ± 0.16	6.06 ± 0.69	5.73 ± 0.88
Intestine	3.9 ± 0.31	3.57 ± 0.46	3.94 ± 0.83	1.85 ± 0.41	1.94 ± 0.14
Stomach	2.47 ± 0.29	2.79 ± 0.67	2.35 ± 0.54	1.53 ± 0.21	1.28 ± 0.1
Brain	0.92 ± 0.26	0.55 ± 0.07	0.56 ± 0.16	0.18 ± 0.05	0.12 ± 0.03
Pancreas	2.38 ± 0.46	1.90 ± 0.14	1.71 ± 0.11	1.28 ± 0.34	1.61 ± 0.59
Tumor /Blood ratio	0.15 ± 0.06	0.64 ± 0.12*	0.33 ± 0.03	3.18 ± 0.40	5.9 ± 2.01
Tumor /Muscle ratio	4.09 ± 2.52	11.12 ± 1.08*	4.2 ± 1.6	15.82 ± 5.41	16.89 ± 4.67

*$P < 0.05$, compared with 4 h.